Enhanced laser-driven proton acceleration using ultrasmall nanoparticles

S. Vallières,[1,2] M. Barberio,[1] M. Scisciò,[1] E. d'Humières,[2] and P. Antici[1]
[1]*INRS-EMT, 1650 boulevard Lionel-Boulet, Varennes (Quebec), J3X 1P7, Canada*
[2]*Centre Lasers Intenses et Applications, Université de Bordeaux, Talence, 33405, France*

(Received 22 January 2019; published 26 September 2019)

An efficient way to enhance laser-driven proton acceleration is by increasing the laser-to-target energy transfer, which can be obtained using nanostructured target surfaces. In this paper, we show that inexpensive and easily producible solid target nanostructuration using ultrasmall nanoparticles having 10 nm in diameter exhibits a nearly twofold maximum proton energy and proton number enhancement. Results are confirmed by particle-in-cell simulations, for several laser pulse lengths. A parameter scan analyzing the effect of the nanoparticle diameter and space gap between the nanospheres shows that the gap has a stronger influence on the enhancement mechanism than the sphere diameter.

DOI: 10.1103/PhysRevAccelBeams.22.091303

Laser-driven proton acceleration, as obtained by the interaction of a high-intensity laser with a target, is a growing field of interest, in particular, for the different potential applications that are consolidating or emerging. These applications include their use in ultrafast radiography [1], novel fusion schemes [2], high-energy density matter [3], laboratory astrophysics [4], medical applications [5–7], novel neutron sources [8], cultural heritage [9,10], using them as injectors for larger accelerators [11,12], and material science [13–16]. Many of these applications build on the routine production of protons, where one of the main challenges is to optimize the proton energy and yield given specific laser parameters. The most common proton acceleration mechanisms that is obtained on typical commercially available multihundred terawatt laser systems is the so-called target-normal sheath acceleration (TNSA) [17], in which protons are accelerated at the rear target surface of a solid foil (target), typically made of Au, Ag, Al, or CH, that is irradiated by a high-intensity ($I > 10^{18}$ W/cm^2), short pulse ($t < 1$ ps) laser operating at wavelengths around 800–1056 nm. In this context, the laser-to-target absorption, i.e., how much energy is transferred from the laser to the target and from there to the particles, is a crucial parameter, since it allows improving the efficiency of the acceleration mechanism. Currently, this efficiency is at most in the order of a few or tens of percent and depends on the target and its structure.

Several attempts have been made to use different kinds of targets, such as to optimize the mean energy, collimation, and number of energetic ("hot") electrons that drive the proton acceleration mechanisms, since, generated at the target front by the ponderomotive force, they travel through the target bulk and establish at its rear surface the electrostatic field that enables the acceleration process [18,19]. In this scenario, several groups demonstrated, both theoretically [20–22] and then experimentally, that the use of nanostructured targets could enhance the absorption of the laser pulse, e.g., by using elliptical Cu nanoparticles in the tens of nanometers size—but irradiated at lower intensities ($I = 10^{15}$–10^{17} W/cm^2) [23]—or using hundreds of nanometer-size Mylar spheres [24,25]. The use of gold nanoparticles in the tens and hundreds of nanometers has also been tested on other (longer pulse) facilities or in an embedded scenario, resulting in increased absorbance even in these conditions [26,27]. Additional effort is put in improving the laser-to-target absorption using various target nanostructuration techniques [24,28–30], such as low-density target foams [31,32], bacteria [33], parabolic structures [34], or nanowires [35]. One of the main disadvantages of the proposed enhancement solutions is that they typically require complex manufacturing or implementation methods, and often their efficiency is strongly dependent on stringent target alignment conditions, making them a less favorable candidate for inexpensive use in high-repetition rate systems. In this paper, we demonstrate that the use of front surface nanostructured targets in the <100 nm range, irradiated with intensity $>10^{18}$ W/cm^2, strongly enhances the laser-to-proton energy transfer and the proton yield. Compared to existing nanostructured targetry, our targets have the advantage of being cheap, easy to manufacture and, thus, easy to implement on higher-repetition rate systems without many constraints. We also show that the gap spacing between the nanostructures is an influential parameter that determines the absorption efficiency in the laser-interaction process. Particle-in-cell (PIC) simulations confirm our

findings. The experiments were performed on the TITAN laser of the Jupiter Laser Facility (JLF) in Livermore, USA, and on the ELFIE laser of the Laboratoire pour l'Utilisation des Lasers Intenses (LULI) in Palaiseau, France. The laser parameters were, respectively, for the TITAN laser an energy $E \sim 220$ J, pulse duration $\tau = 700$ fs, and central wavelength $\lambda_0 = 1.054$ μm and for the ELFIE laser an energy $E \sim 12$ J, pulse duration $\tau = 350$ fs, and central wavelength $\lambda_0 = 1.057$ μm. Both lasers were focused down by an $f/3$ off-axis parabola to about 8–10 μm focal spot diameter (FWHM), yielding an intensity $I \sim 3 \times 10^{19} - 5 \times 10^{20}$ W/cm^2 on target. The laser was irradiating with normal incidence the different targets [for the setup, see Fig. 1(a)]. The amplified spontaneous emission (ASE) has been measured to be $<10^{-6}$ in contrast in both cases. The proton beam spectrum was monitored by placing two Thomson parabolas, respectively, at 0° and 16° for the TITAN laser and 0° and 9° for the ELFIE laser with respect to the normal direction from the proton source. Additional information about the proton beam was retrieved using radiochromic films [36]. The nanostructured targets were produced by spray drying different layers of in-house-produced gold or silver nanoparticles (NPs) with a diameter of 10 nm onto a solid aluminum target with thickness 15 μm [37,38] [for an image of the produced NPs, see Fig. 1(b)]. We considered this target material since it is one of the most used and cheapest target materials in laser-driven proton acceleration, was producing the best results compared to other materials and thicknesses when used as a proton source [13,39], and the wetting properties between them and the gold or silver NPs can ensure the realization of a uniform nanostructured film on the surface with limited aggregation of nanoparticles [40]. As shown in Fig. 1(b), NPs can aggregate locally on the surface, which changes the effective gap parameter of the nanostructuration. The latter is a linear combination of the different gap space that the laser encounters in its focal spot when hitting the target. With this technique, we were able to generate targets that have simultaneously high light absorption, high roughness, and low cost. The low fabrication costs of all nanostructured films result from a simple process combination of laser ablation synthesis in solution for the production of the NPs of different sizes [41] and spray dry of the solution onto planar surfaces, which enhances the surface roughness.

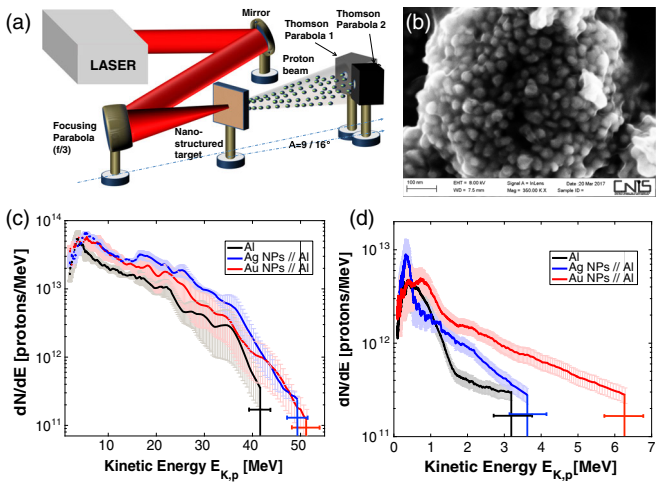

FIG. 1. (a) Experimental setup. (b) Scanning electron microscope (SEM) image of gold NPs deposited onto a planar 15 μm Au foil target. (c) Proton spectra with error bars obtained on the TITAN laser with Ag (blue curve) and Au NPs (red curve) on Al foils compared to a standard 15 μm Al foil (black curve). (d) Proton spectra obtained on the ELFIE laser with Ag (blue curve) and Au NPs (red curve) on Al foils compared to a standard 15 μm Al foil (black curve).

Figures 1(c) and 1(d) show the proton spectra obtained for nanostructured aluminum targets as produced on the TITAN and ELFIE lasers, each spectrum representing a five-shot average along with its standard error bars. As one can see, all nanostructured targets perform better than the solid targets for both the maximum proton energy and proton number. Regarding the TITAN laser, we find an enhancement of 79% and 51% in the proton yield, as obtained by integrating the number of protons between 1 MeV and the maximum proton energy, and an enhancement of 19% and 23% in the maximum proton energy, for Ag NPs deposited on Al foils (AgNPs//Al) and AuNPs//Al, respectively. Similarly, we obtain for the ELFIE laser a proton yield enhancement of 67% and 190% in the proton yield and a maximum proton energy enhancement of 13% and 97% for AgNPs//Al and AuNPs//Al, respectively. For both lasers, the use of Au nanoparticles seems preferable to the use of Ag particles. The higher atomic number of gold indeed provides greater electron density in the accelerating hot electron sheath, thus giving a higher proton number and energies.

We run PIC simulations to shed light onto the underlying acceleration process and confirm the optimized conditions. PIC [42] simulations were performed using the 2D3V PICLS code using a Gaussian p-polarized normally incident laser pulse with a peak intensity of 5×10^{20} W/cm^2 ($a_0 = 15$, the normalized intensity of the vector potential). Two sets of simulations were developed, the first one consisting in varying the pulse length duration $\tau = 25$, 100, 200, and 300 fs at full width at half maximum (FWHM) on the target. Given the nanometric matrix of the target, we used highly resolved spatial steps of $dx = dy = 2$ nm, leading to temporal steps of $dt = 6.6$ as. Concerning the box size, a plane-wave approximation with periodic boundaries in the transverse direction was used to compensate the strong computing time limitation from the small pixel size [for the setup of the simulation box, see Fig. 3(a)]. The box size was 24200×420 pixels ($30\lambda_0 \times 1\lambda_0$) in the longitudinal and transverse axes, respectively, with 20 particles per pixel. The target was made of a layer of gold spheres with diameter d_{NP} of 20 nm placed side by side, on a 500-nm-thick gold foil ($2500n_c$, where n_c is the critical density). At

the rear side of the target was placed a 20 nm layer of protons ($15n_c$), representing water and hydrocarbon contaminants on the surface, and simulations were run for 600 fs. The second set of simulations consisted in varying NP diameters in the range of 5–100 nm as well as the space gap g between NPs in the range of 0–400 nm. To achieve a good resolution of NPs smaller in size, we decreased the pixel size to 1 nm. To compensate the highly demanding computing power of these simulations, the box size was reduced to 11200×800 pixels ($14\lambda_0 \times 1\lambda_0$) and the simulation time to 200 fs, with a pulse duration of 25 fs. In order to optimize the computational burden, we first verified for a few pulse lengths that the results obtained using the shorter pulse (25 fs) were consistent for those obtained using longer pulses (>300 fs), the latter simulations being far more computationally demanding. The results are presented in Fig. 2. In Figs. 2(a) and 2(b), we can note the continuously increasing laser energy absorption and maximum proton kinetic energy in this pulse duration range. Small NPs of 20 nm in diameter do provide a considerable gain for both parameters, reaching an enhancement ratio of roughly 50% even for long pulse durations of hundreds of femtoseconds [see Fig. 2(c)], which is consistent with experimental enhancements observed in Fig. 1. This particular enhancement seem to flatten off for long pulses, although for a short pulse (25 fs) the maximum energy gain reaches over 250%. Even if small NPs of 20 nm seem to add a negligible thickness over a target with a thickness of 500 nm (which in the PIC simulation was the thickness of the solid target), the simulations still demonstrate a strong enhancement potential for long pulses of a few hundred femtoseconds. Given the many simulations required to do a parameter scanning and the good representation of NP enhancement even with a short pulse, we performed the rest of the simulations using the same on-target intensity but using the shorter laser pulse duration (25 fs) to allow for shorter computation time and knowing that our simulations would only underestimate the phenomena. The short-pulse results are also of interest for the many short-pulse commercial lasers that are currently implementing laser-generated proton acceleration.

At first, we explore the effect of the nanoparticle dimensions on the laser energy absorption 200 fs after the main pulse, which is a sufficiently long time span to allow for saturation of the acceleration process [see Fig. 3(b)]. We clearly observe a rapid absorption enhancement for increasing nanoparticle diameters ranging from 5 to 20 nm (the 0 nm size representing the solid target), while after this dimension the absorption only minimally improves, almost coming to saturation. This reflects on the simulated electron spectra taken 20 fs after the interaction (where this time interval has been chosen since at this time span most energy is transferred to the electrons) [see Fig. 3(c)], where we note that the maximum kinetic energy of the electrons more than doubles when using 10–60 nm nanoparticles compared to a flat target. We also observe that the number of electrons increases similarly to the maximum energy. The surface density of the NPs is very likely to play a central role in this enhancement, which is not solely provoked from the NP diameter, suggesting a strong importance of the number and size of gaps between NPs rather than just the NP dimension. Our findings are supported by the analysis of the longitudinal electric field produced at the target rear surface at the time 20 fs after the impact [see Fig. 3(d)]. We see that the electric field at the target rear surface increases almost proportionally to the maximum electron energy enhancement up to a nanoparticle size of 10 nm and then stabilizes between 10 and 60 nm. After this particle size, the position of the field shifts away from the rear target surface, thus lowering its effect on the acceleration process, and finally climbs up again for 100 nm particles. The increasing trend of the electrons' maximum energy in Fig. 3(c) follows the same pattern as in Fig. 3(d), denoting well the electron-dependent behavior of the accelerating field.

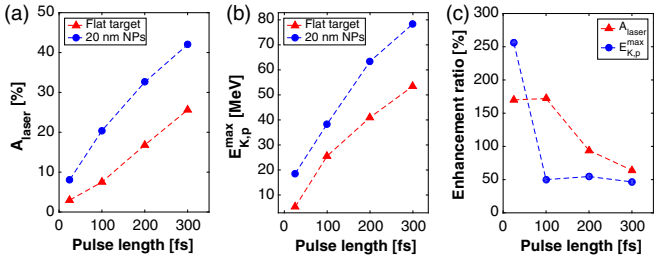

FIG. 2. Pulse length effect on total laser energy absorption A_{laser} from the target (a) and on the maximum kinetic energy gained by protons $E_{K,p}{}^{\max}$ (b). The enhancement ratio for both parameters is also shown in (c).

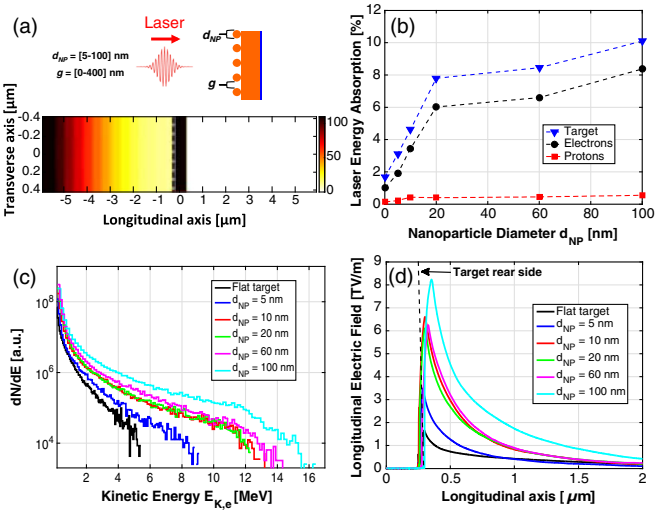

FIG. 3. (a) Schematic geometry of the PIC simulations. (b) Laser energy absorption for different nanoparticle diameters, comparing energy absorption from the whole target (blue triangles), from electrons (black circles) and from protons (red squares). (c) Hot electron spectra for different nanoparticle diameters. (d) Mean longitudinal electric field at a central radial position.

In Fig. 4(a), we show the respective proton spectra for different NP diameters d_{NP}, where the maximum energy axis has been normalized to the maximum proton energy obtained with the solid target. One can see that an increase in the laser energy absorption significantly increases the maximum achievable proton energy, up to a nearly fourfold increase, in line with the experimental results. In order to investigate the importance of the gap g between the nanospheres, we fixed the NP diameter at 10 nm, our experimental working point, and changed the gap g in the range 0–400 nm [see Fig. 4(b)]. We can clearly note that the gap opening plays a stronger role than varying the nanoparticle diameter: When separating the nanoparticles by a gap of 10 nm, simulations show that the maximum proton energy enhancement is much more pronounced than when using 100 nm diameter nanoparticles but with gap distance $g = 0$ nm. This is because the ejected electrons from the NPs can accelerate in the laser field while traveling in the gap space before passing through the target bulk, where the electric field is nearly zero for dense plasmas. The gap region allows for greater electron heating and, therefore, stronger laser energy absorption, a consistent conclusion to those presented in the paper of Blanco *et al.* [21], where a theoretical study with triangular nanostructures shows that this phenomenon is due to the relativistic electron trajectory in the gap space. This is a different but complementary trend when compared to several other papers using targets nanostructured with nanoparticles, where the nanospheres are always tightly packed (i.e., $g = 0$) [22–24]. The aforementioned papers foresee a nearly absent improvement in the acceleration regime for NPs with a diameter of 10 nm. Our results indicate that the gap distance plays a stronger role than the diameter size. This effect is more pronounced for smaller NPs, since they allow for a greater amount of gap space. We also see that there is an increasing trend for larger gaps, up to gap sizes of 100 nm, most likely since up to those gap distances this phenomenon is enhanced. For a gap distance of $g = 400$ nm (magenta curve), the enhancement is still present but the trend is reverting. At this larger gap size, the effect of the nanoparticles is reduced, and we are returning back towards the flat target case (i.e., $E_{K,\mathrm{cutoff}}^{\mathrm{flat}} < E_{K,\mathrm{cutoff}}^{g=400\ \mathrm{nm}} < E_{K,\mathrm{cutoff}}^{g=100\ \mathrm{nm}}$). The cutoff energy enhancement is maximized for a gap g of 100 nm, reaching a sevenfold increase, much higher than the fourfold obtained by varying the NP diameter d_{NP}. This suggests that, when using nanoparticle-enhanced targets, it is preferable to have larger gap spaces (about $g = 100$ nm) with many small NPs ($d_{\mathrm{NP}} < 100$ nm) rather than tightly packed ($g = 0$) large NPs ($d_{\mathrm{NP}} > 100$ nm). Indeed, having smaller NPs provides the possibility to have greater NP surface densities and, hence, greater gap densities, rather than solely relying on the NPs diameter. Moreover, in the presented PIC simulations, the NPs are all equally spaced with a single gap value, whereas the experimental targets have a random distribution of gap spaces. Hence, the optimum experimental condition strongly depends on the effect of several gap distances, which explains the strong cutoff energy increase seen experimentally. Concerning the thickness of the NP layer, as shown in the paper of Barberio *et al.* [35] detailing the present nanostructured target fabrication methodology, the NPs are dried on a flat target until the surface roughness saturates, adding at most several tens of nanometers on the initial flat target surface (NPs multilayer), hence making the thickness of the nanostructured layer negligible compared to the total thickness. The substrate thickness (as long as the target remains opaque to the laser, which is the case in our simulations) has an influence on the absolute cutoff energy but not on the relative increase when comparing targets with and without nanospheres. The important factor here is the increased transverse density variations (given by the increased surface roughness) rather than the target thickness variation. This enhancement process is dependent on an increased density of hotter electrons at the rear side of the target, as shown in Fig. 3, which ultimately leads to a stronger TNSA electric field. Having a less dense plasma (produced by higher absorption through an increased surface roughness) at the target front allows one to reduce the reflection coefficient of the target and, thus, increases the energy absorption from the incident wave, compared to the flat target case. Details about the modifications of the nanospheres when the impinging laser reaches the peak intensity are thus not a necessary requirement for this enhancement mechanism as observed in our simulations. The production of a favorable preplasma up to the peak intensity is the key to produce a greater number of hotter electrons, leading to higher kinetic energies of the accelerated protons.

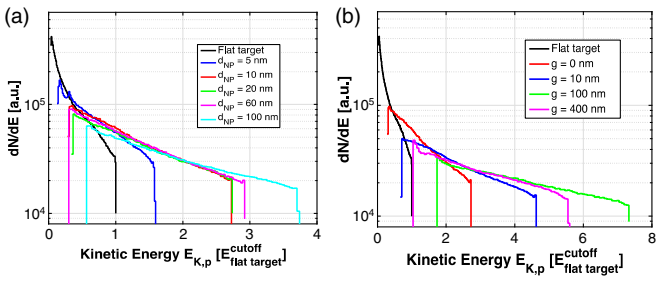

FIG. 4. (a) Proton kinetic energy spectra for different NP diameters d_{NP}—the gap size g between the different nanoparticles is kept at $g = 0$ nm. (b) Influence of the gap size g on the proton spectra—the nanoparticle dimension has been kept fixed at $d_{\mathrm{NP}} = 10$ nm. Since the number of protons in the simulation is fixed and the plane-wave approximation is used, the minimum energy (left cutoff in the spectrum) is shifted with an increasing maximum proton energy. The flat target cutoff normalization energy is 4.5 MeV.

In conclusion, we have shown that nanostructured targets with ultrasmall NPs allow enhancing the laser energy absorption and, thus, increase the maximum proton energy and number. Moreover, we have investigated the effect of the gap parameter g, showing that this parameter has a

stronger enhancement effect on the proton cutoff energy than the diameter of the NPs, reaching a sevenfold increase with gap variation compared to fourfold in tightly packed geometry ($g = 0$). This conclusion differs from other findings published in the literature using nanoparticles for target nanostructuration, where the use of 10 nm NPs should be of negligible importance. Here, we show that ultrasmall NPs provide significant proton energy enhancement, in particular, due to the strong gap opening effect along with a greater gap density provided by small NPs. Compared to existing nanostructured targets that require the use of complex and expensive manufacturing procedures (e.g., lithographic methods), our targets present the advantage of being both simple and inexpensive to manufacture and do not exhibit the stringent laser-matter alignment conditions as required by microstructured targets. These targets are therefore good candidates for being implemented on high-repetition-rate laser-driven proton beam lines, where any efficiency enhancement in the laser-driven acceleration process is of high impact.

We acknowledge the expert support of the TITAN and LULI laser teams and the expertise of F. Mura from the CNIS center. We thank S. Veltri, A. Morabito, K. Nelissen, and J. Fuchs for their precious help and for providing equipment. This work is supported by FRQNT (nouveaux chercheurs, Grant No. 174726, Equipe 2016-PR-189974), the National Sciences and Engineering Research Council of Canada (NSERC) (Discovery Grant No. RGPIN-2018-05772 and the Alexander-Graham-Bell Graduate Scholarship for S. V.), Compute Canada (Job: pve-323-ac, P. A.) as well as the Canada Foundation for Innovation (CFI). The use of the Jupiter Laser Facility was supported by the U.S. Department of Energy, Lawrence Livermore National Laboratory, under Contract No. DE-AC52-07NA27344. Concerning the use of the ELFIE laser facility, we acknowledge support by LASERLAB Europe (Grant Agreement No. 654148 under the European Union's Horizon 2020 research and innovation program). Additional support comes from the EU program HPRI CT 1999-0052, LANL Laboratory Directed Research & Development, corporate support of General Atomics, and UNR Grant No. DE-FC08-01NV14050.

[1] L. Romagnani, J. Fuchs, M. Borghesi, P. Antici, P. Audebert, F. Ceccherini, T. Cowan, T. Grismayer, S. Kar, A. Macchi, P. Mora, G. Pretzler, A. Schiavi, T. Toncian, and O. Willi, Dynamics of Electric Fields Driving the Laser Acceleration of Multi-MeV Protons, Phys. Rev. Lett. **95**, 195001 (2005).

[2] M. Roth, T. E. Cowan, M. H. Key, S. P. Hatchett, C. Brown, W. Fountain, J. Johnson, D. M. Pennington, R. A. Snavely, S. C. Wilks, K. Yasuike, H. Ruhl, F. Pegoraro, S. V. Bulanov, E. M. Campbell, M. D. Perry, and H. Powell, Fast Ignition by Intense Laser-Accelerated Proton Beams, Phys. Rev. Lett. **86**, 436 (2001).

[3] P. K. Patel, A. J. Mackinnon, M. H. Key, T. E. Cowan, M. E. Foord, M. Allen, D. F. Price, H. Ruhl, P. T. Springer, and R. Stephens, Isochoric Heating of Solid-Density Matter with an Ultrafast Proton Beam, Phys. Rev. Lett. **91**, 125004 (2003).

[4] B. Albertazzi *et al.*, Laboratory formation of a scaled protostellar jet by coaligned poloidal magnetic field, Science **346**, 325 (2014).

[5] A. Yogo, T. Maeda, T. Hori, H. Sakaki, K. Ogura, M. Nishiuchi, A. Sagisaka, H. Kiriyama, H. Okada, S. Kanazawa, T. Shimomura, Y. Nakai, M. Tanoue, F. Sasao, P. R. Bolton, M. Murakami, T. Nomura, S. Kawanishi, and K. Kondo, Measurement of relative biological effectiveness of protons in human cancer cells using a laser-driven quasi-monoenergetic proton beamlineAppl. Phys. Lett. **98**, 053701 (2011).

[6] J. Metzkes, T. E. Cowan, L. Karsch, S. D. Kraft, J. Pawelke, C. Richter, T. Richter, K. Zeil, and U. Schramm, Preparation of laser-accelerated proton beams for radiobiological applications, Nucl. Instrum. Methods Phys. Res., Sect. A **653**, 172 (2011).

[7] D. Doria, K. F. Kakolee, S. Kar, S. K. Litt, F. Fiorini, H. Ahmed, S. Green, J. C. G. Jeynes, J. Kavanagh, D. Kirby, K. J. Kirkby, C. L. Lewis, M. J. Merchant, G. Nersisyan, R. Prasad, K. M. Prise, G. Schettino, M. Zepf, and M. Borghesi, Biological effectiveness on live cells of laser driven protons at dose rates exceeding 109 Gy/s, AIP Adv. **2**, 011209 (2012).

[8] M. Roth *et al.*, Bright Laser-Driven Neutron Source Based on the Relativistic Transparency of Solids, Phys. Rev. Lett. **110**, 044802 (2013).

[9] M. Barberio, S. Veltri, M. Scisciò, and P. Antici, Laser-accelerated proton beams as diagnostics for cultural heritage, Sci. Rep. **7**, 40415 (2017).

[10] M. Barberio and P. Antici, Laser-PIXE using laser-accelerated proton beams, Sci. Rep. **9**, 6855 (2019).

[11] P. Antici, M. Fazi, A. Lombardi, M. Migliorati, L. Palumbo, P. Audebert, and J. Fuchs, Numerical study of a linear accelerator using laser-generated proton beams as a source, J. Appl. Phys. **104**, 124901 (2008).

[12] P. Antici, M. Migliorati, A. Mostacci, L. Picardi, L. Palumbo, and C. Ronsivalle, A compact post-acceleration scheme for laser-generated protons, Phys. Plasmas **18**, 073103 (2011).

[13] M. Barberio, S. Vallières, M. Scisciò, G. Kolhatkar, A. Ruediger, and P. Antici, A compact post-acceleration scheme for laser-generated protons, Carbon **139**, 531 (2018).

[14] M. Barberio, M. Scisciò, S. Vallières, F. Cardelli, G. Famulari, T. Gangolf, G. Revet, M. Senzaqua, S. N. Chen, A. Schiavi, and P. Antici, Laser-accelerated particle beams for stress testing of materials, Nat. Commun. **9**, 372 (2018).

[15] M. Barberio, M. Scisciò, S. Vallières, S. Veltri, A. Morabito, and P. Antici, Laser-generated proton beams for high-precision ultra-fast crystal synthesis, Sci. Rep. **7**, 12522 (2017).

[16] M. Barberio, S. Veltri, M. Scisciò, and P. Antici, Laser-Accelerated Proton Beams as Diagnostics for Cultural Heritage, Sci. Rep. **7**, 40415 (2017).

[17] S. C. Wilks, W. L. Kruer, M. Tabak, and A. B. Langdon, Absorption of Ultra-Intense Laser Pulses, Phys. Rev. Lett. **69**, 1383 (1992).

[18] L. Cao, Y. Gu, Z. Zhao, L. Cao, W. Huang, W. Zhou, X. T. He, W. Yu, and M. Y. Yu, Control of the hot electrons produced by laser interaction with nanolayered target, Phys. Plasmas **17**, 103106 (2010).

[19] P. Antici, J. Fuchs, M. Borghesi, L. Gremillet, T. Grismayer, Y. Sentoku, E. d'Humières, C. A. Cecchetti, A. Mancic, A. C. Pipahl, T. Toncian, O. Willi, P. Mora, and P. Audebert, Hot and Cold Electron Dynamics Following High-Intensity Laser Matter Interaction, Phys. Rev. Lett. **101**, 105004 (2008).

[20] A. Andreev, N. Kumar, K. Platonov, and A. Pukhov, Efficient generation of fast ions from surface modulated nanostructure targets irradiated by high intensity short-pulse lasers, Phys. Plasmas **18**, 103103 (2011).

[21] J. Yu, Z. Zhao, X. Jin, F. Wu, Y. Yan, W. Zhou, L. Cao, B. Li, and Y. Gu, Laser-driven proton acceleration using a conical nanobrush target, Phys. Plasmas **19**, 053108 (2012).

[22] M. Blanco, M. T. Flores-Arias, C. Ruiz, and M. Vranic, Table-top laser-based proton acceleration in nanostructured targets, New J. Phys. **19**, 033004 (2017).

[23] S. Bagchi, P. Prem Kiran, M. K. Bhuyan, S. Bose, P. Ayyub, M. Krishnarmurthy, and G. R. Kumar, Fast ion beams from intense, femtosecond laser irradiated nano-structured surfaces, Appl. Phys. B **88**, 167 (2007).

[24] D. Margarone, O. Klimo, I. J. Kim, J. Prokupek, J. Limpouch, T. M. Jeong, T. Mocek, J. Psikal, H. T. Kim, J. Proska, K. H. Nam, L. Stolcova, I. W. Choi, S. K. Lee, J. H. Sung, T. J. Yu, and G. Korn, Laser-Driven Proton Acceleration Enhancement by Nanostructured Foils, Phys. Rev. Lett. **109**, 234801 (2012).

[25] O. Klimo, J. Psikal, J. Limpouch, J. Proska, F. Novotny, T. Ceccotti, V. Floquet, and S. Kawata, Short pulse laser interaction with micro-structured targets: simulations of laser absorption and ion acceleration, New J. Phys. **13**, 053028 (2011).

[26] L. Torrisi, L. Calcagno, M. Cutroneo, J. Badziak, M. Rosinski, A. Zaras-Szydlowska, and A. Torrisi, Nanostructured targets for TNSA laser ion acceleration, Nukleonika **61**, 103 (2016).

[27] L. Torrisi, Ion acceleration from intense laser-generated plasma: methods, diagnostics and possible applications, Nukleonika **60**, 207 (2015).

[28] H. Schwoerer, S. Pfotenhauer, O. Jäckel, K.-U. Amthor, B. Liesfeld, W. Ziegler, R. Sauerbrey, K. W. D. Ledingham, and T. Esirkepov, Laser-plasma acceleration of quasi-monoenergetic protons from microstructured targets, Nature (London) **439**, 445 (2006); S. Okihara, T. Zh. Esirkepov, K. Nagai, S. Shimizu, F. Sato, M. Hashida, T. Iida, K. Nishihara, T. Norimatsu, Y. Izawa, and S. Sakabe, Ion generation in a low-density plastic foam by interaction with intense femtosecond laser pulses, Phys. Rev. E **69**, 026401 (2004); J. Zhang, Y. T. Li, Z. M. Sheng, Y. Y. Ma, Z. Jin, Z. L. Chen, R. Kodama, T. Matsuoka, M. Tampo, K. A. Tanaka, T. Tsutsumi, and T. Yabuuchi, Bulk acceleration of ions in intense laser interaction with foams, Plasma Phys. Controlled Fusion **47**, B879 (2005).

[29] M. Cutroneo, L. Torrisi, L. Calcagno, and A. Torrisi, Characterization of thin films for TNSA laser irradiation, J. Phys. Conf. Ser. **508**, 012012 (2014).

[30] L. Willingale, S. R. Nagel, A. G. R. Thomas, C. Bellei, R. J. Clarke, A. E. Dangor, R. Heathcote, M. C. Kaluza, C. Kamperidis, S. Kneip, K. Krushelnick, N. Lopes, S. P. D. Mangles, W. Nazarov, P. M. Nilson, and Z. Najmudin, Characterization of High-Intensity Laser Propagation in the Relativistic Transparent Regime through Measurements of Energetic Proton Beams, Phys. Rev. Lett. **102**, 125002 (2009).

[31] M. Passoni, A. Sgattoni, I. Prencipe, L. Fedeli, D. Dellasega, L. Cialfi, Il Woo Choi, I. Jong Kim, K. A. Janulewicz, H. W. Lee, J. H. Sung, S. K. Lee, and C. H. Nam, Toward high-energy laser-driven ion beams: Nanostructured double-layer targets, Phys. Rev. Accel. Beams **19**, 061301 (2016).

[32] P. Antici, J. Fuchs, E. d'Humieres, J. Robiche, E. Brambrink, S. Atzeni, A. Schiavi, Y. Sentoku, P. Audebert, and H. Pepin, Laser acceleration of high-energy protons in variable density plasmas, New J. Phys. **11**, 023038 (2009).

[33] M. Dalui, M. Kundu, S. Tata, A. D. Lad, J. Jha, K. Ray, and M. Krishnamurthy, Novel target design for enhanced laser driven proton acceleration, AIP Adv. **7**, 095018 (2017).

[34] A. Lübcke, A. A. Andreev, S. Höhm, R. Grunwald, L. Ehrentraut, and M. Schnürer, Prospects of target nanostructuring for laser proton acceleration, Sci. Rep. **7**, 44030 (2017).

[35] M. A. Purvis, V. N. Shlyaptsev, R. Hollinger, C. Bargsten, A. Pukhov, A. Prieto, Y. Wang, B. M. Luther, L. Yin, S. Wang, and J. J. Rocca, Relativistic plasma nanophotonics for ultrahigh energy density physics, Nat. Photonics **7**, 796 (2013).

[36] S. Vallières, C. Bienvenue, P. Puyuelo-Valdes, M. Salvadori, E. d'Humières, F. Schiettekatte, and P. Antici, Low-energy proton calibration and energy-dependence linearization of EBT-XD radiochromic films, Rev. Sci. Instrum. **90**, 083301 (2019).

[37] M. Barberio, M. Scisciò, S. Veltri, and P. Antici, Fabrication of nanostructured targets for improved laser-driven proton acceleration, Superlattices Microstruct. **95**, 159 (2016).

[38] S. Vallieres, A. Morabito, S. Veltri, M. Sciscio, M. Barberio, and P. Antici, Laser-driven proton acceleration with nanostructured targets, SPIE Opt. Optoelectron. **10240**, 1024009 (2017).

[39] M. Gauthier, A. Lévy, E. d'Humières, M. Glesser, B. Albertazzi, C. Beaucourt, J. Breil, S. N. Chen, V. Dervieux, J. L. Feugeas, P. Nicolaï, V. Tikhonchuk, H. Pépin, P. Antici, and J. Fuchs, Investigation of longitudinal proton acceleration in exploded targets irradiated by intense short-pulse laser, Phys. Plasmas **21**, 013102 (2014).

[40] M. Barberio, F. Stranges, and F. Xu, Coating geometry of Ag, Ti, Co, Ni, and Al nanoparticles on carbon nanotubes, Appl. Surf. Sci. **334**, 174 (2015).

[41] M. Barberio and P. Antici, In situ study of nucleation and aggregation phases for nanoparticles grown by laser-driven methods, Sci. Rep. **7**, 41372 (2017).

[42] Y. Sentoku and A. J. Kemp, Numerical methods for particle simulations at extreme densities and temperatures: Weighted particles, relativistic collisions and reduced currents, J. Comput. Phys. **227**, 6846 (2008).